

# Evanescent waves in microscopy

Matthias Kramer, Carl Zeiss, Göttingen, Germany

In recent years microscopy has experienced a Renaissance brought about by the widespread acceptance of fluorescently labelling biological samples. Using protein-like dyes the smallest cell and tissue structures can be visualized and made visible with the help of appropriate filters in a fluorescence microscope.

Utilizing the confocal principle, high resolution along the Z-axis (in z-direction) can be achieved within the object. Recently several methods were also established in the market of widefield microscopy, which make an improvement of the z-resolution possible. Beside the method of grating projection [1] now TIRF microscopy (TIRF – Total Internal Reflection Fluorescence, [2,3]) has also become widely accepted for imaging applications [4].

## 1 The appeal of low penetration depths

In contrast to confocal detection TIRF is limited to imaging the boundary surface between cover glass and sample. The z-focus cannot be shifted. Nevertheless one can vary the penetration depth of the evanescent field in a small range by changing the angle of incidence of the excitation light and can therefore collect images with different section thicknesses. **Figure 1** shows the impressive improvement in contrast the TIRF effect delivers: left hand side of the figure a cell in conventional fluorescence microscopy (Epi fluorescence), on the right hand side the same object in TIRF [4]. Here structures become visible, which are up to 100-200 nm away from the interface of the cover glass and sample. More deeply located structures are barely excited due to the exponential decay of the evanescent field. The associated paths of rays are indicated in **figure 2**.

## 2 Basics of evanescent waves

The principle of TIRF microscopy is based on the generation of an evanescent (lat. evanescere = "vanish" or "fade away") wave at the interface of two media with different refractive index. While the exact solution of the wave equation for evanescent waves is cited frequently in the literature, their detailed derivation in con-

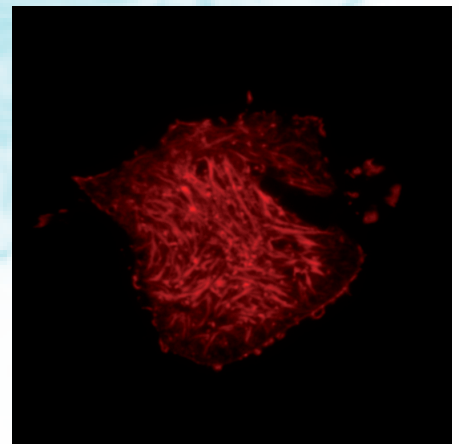
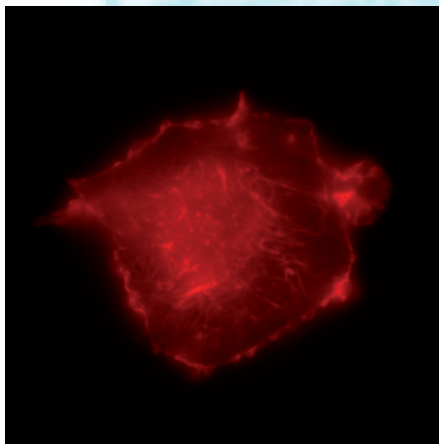


**Figure 1:** Phalloidin f-Actin protein coupled with Alexa (546), actin filaments, Cytoskeleton within the range of the Submembrane cortex in cattle cells, left in Epifluorescence, right in TIRF (Dr. J. Klingauf, MPI for biophysical chemistry, Goettingen)

nection with TIRF was not described and is indicated in the following. To homogeneous, isotropic and dispersive media the Helmholtz equation deduced from the general wave equation applies

$$\Delta \vec{E}(\vec{r}, \omega) + \frac{\omega^2}{c^2} \epsilon(\omega) \vec{E}(\vec{r}, \omega) = 0 \quad (\text{Eq. 1})$$

who's solution can be written as

$$\vec{E}(\vec{r}, \omega) = \vec{E}(\vec{k}, \omega) e^{i\vec{k}\vec{r}} \quad (\text{Eq. 2})$$

Here is E the electrical field strength, r the radius vector,  $\omega$  the circular frequency and k the generally complex propagation vector of the wave. The corresponding dispersion relation is described by

$$\vec{k}^2 = \frac{\omega^2}{c^2} \epsilon(\omega) \quad (\text{Eq. 3})$$

with c being the speed of light. The typical slope of the dielectric function in optical media is shown in **figure 3**. In ranges "1" and "2" the real part  $\epsilon'$  of the dielectric function largely exceeds the imaginary part  $\epsilon''$ . In these ranges the following relation is valid

$$\begin{aligned} \epsilon' \gg \epsilon'' > 0 &\rightarrow \vec{k}^2 = (\vec{k}' + i\vec{k}'')^2 \\ &= \vec{k}'^2 - \vec{k}''^2 + 2i\vec{k}'\vec{k}'' \cong \frac{\omega^2}{c^2} \epsilon'(\omega) > 0 \end{aligned} \quad (\text{Eq. 4})$$

Here special solutions for the Helmholtz equation can be found. For the case  $\vec{k}'' = 0$  one speaks of polaritons, which are not to be regarded closer. In the case  $\vec{k}' \perp \vec{k}''$  a wave absorbed transverse to its direction of propagation  $\vec{k}'$  results:

$$\vec{E}(\vec{r}, \omega) = \vec{E}(\vec{k}, \omega) e^{i\vec{k}'\vec{r}} e^{-\vec{k}''\vec{r}} \quad (\text{Eq. 5})$$

This is a so-called evanescent or inhomogeneous wave, whose surfaces of constant phase and surfaces of constant amplitude are perpendicular to each other.

## 3 Evanescent waves at a plane interface

We regard the boundary surface of two optically transparent media with refractive index  $n_1$  and  $n_2$ , whereby  $n_1 > n_2$ . An incident light-ray  $\vec{k}_i$  is refracted at the interface and deviates further away from the normal (**figure 4**).

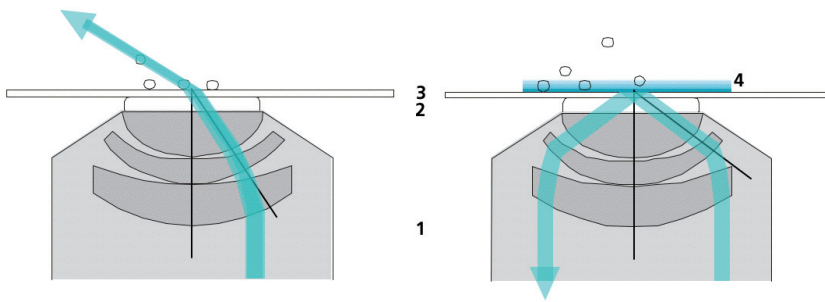


**Figure 2:** TIRF microscopy inside an objective, on the left of the schematic the representation of the beampath below the critical angle, right under the conditions of the total reflection (1: Objective, 2: Immersion liquid; 3: Cover glass, 4: evanescent field)

With an E vector polarized in y direction ("p-polarized")

$$\vec{k}_2 = \vec{k}_2' + \vec{k}_2'' \rightarrow \vec{k}_2' = \begin{pmatrix} k_{2x}' \\ 0 \\ 0 \end{pmatrix}, \vec{k}_2'' = \begin{pmatrix} 0 \\ 0 \\ k_{2z}'' \end{pmatrix}, \vec{e}_y = \begin{pmatrix} 0 \\ 1 \\ 0 \end{pmatrix} \quad (\text{Eq. 6})$$

the solution of the Helmholtz equation can be written as:

$$\vec{E}(\vec{r}, \omega) = \vec{e}_y E_y(\vec{k}_2, \omega) e^{ik_{2x}'x} e^{-k_{2z}''z} \quad (\text{Eq. 7})$$

Particularly

$$\vec{k}_2'^2 = \vec{k}_2'^2 - \vec{k}_2''^2 > 0 \rightarrow k_{2x}' \geq k_2 \quad (\text{Eq. 8})$$

results which as a result of

$$k_{2x}' = k_{1x} = \frac{2\pi}{\lambda_0} n_1 \sin(\alpha_1) \geq \frac{2\pi}{\lambda_0} n_2 = k_2 \quad (\text{Eq. 9})$$

$$\rightarrow n_1 \sin(\alpha_1) \geq n_2$$

is the condition for total reflection for the angle of incidence  $\alpha_1$  of both media at their interface. The evanescent wave is generated only at the condition of total reflection.

If no absorbing medium is beyond the interface, the reflected wave does not

suffer loss of energy. When fluorescent dyes are present they become excited at expense of the reflected wave.

#### 4 The role of the penetration depth

With Snell's law the intensity of the evanescent field can be written as

$$I(\vec{r}, \omega) = \vec{E}^2(\vec{r}, \omega) \sim I(0) e^{-z/\delta} \quad (\text{Eq. 10})$$

where

$$\delta = \frac{\lambda_0}{4\pi n_2 \sqrt{[\sin(\alpha_1)/\sin(\alpha_g)]^2 - 1}} \quad (\text{Eq. 11})$$

is the penetration depth of the evanescent field and  $\alpha_g$  is the critical angle of total reflection. Typical values in TIRF microscopy are

$$\lambda_0 = 488 \text{ nm}, n_1 = 1.518, n_2 = 1.33 \rightarrow \alpha_g = 61.2^\circ$$

The penetration depth  $\delta$  versus the angle

of incidence  $\alpha_1$  can be plotted, see **figure 5**.

At the critical angle  $\alpha_g$  of total reflexion the penetration depth has a singularity, which becomes apparent in practice as transition to the "normal" Epi fluorescence illumination. Here the volume lit up in the sample corresponds to the waist volume of the path of rays behind the objective.

The shaded area in figure 5 represents the working range of the high aperture Zeiss objective used for the TIRF effect in figure 1 (NA = 1.45). It is downward limited by the critical angle of total reflection determined by the optical properties of the cover glass and the aqueous medium of the sample ( $\alpha_g=61,2^\circ$ ). Due to the divergence of the laser in the entrance aperture of the objective this angle range is reduced further. In test measurements with fluorescent Latex beads of 4-6  $\mu\text{m}$  diameter ("microbeads") penetration depths of 125 nm were experimentally proven.

One must point out that the term "TIRF

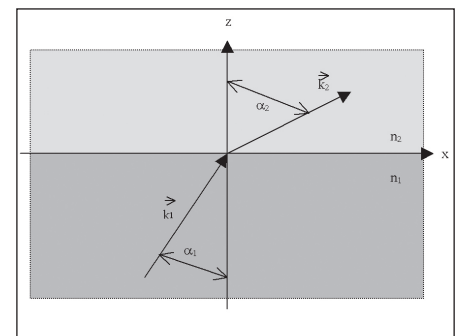


**Figure 4:** Scheme of refraction of light at the interface of two optical media with refractive indices  $n_1$  and  $n_2$

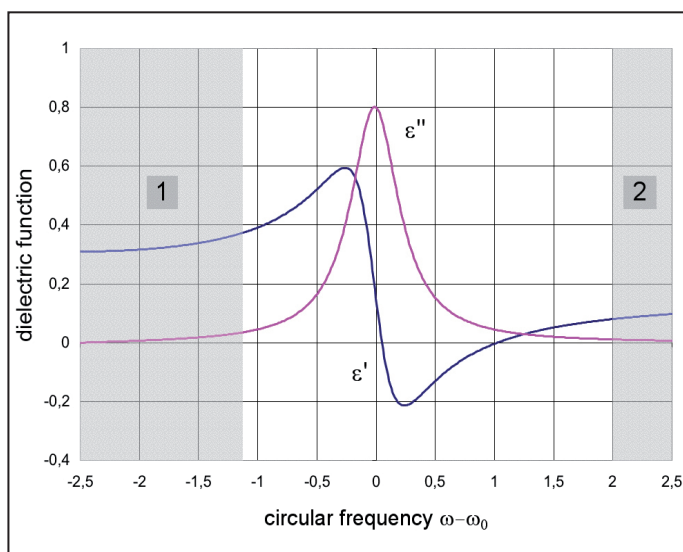


**Figure 3:** Typical slope of the dielectric function within the range of an absorption line

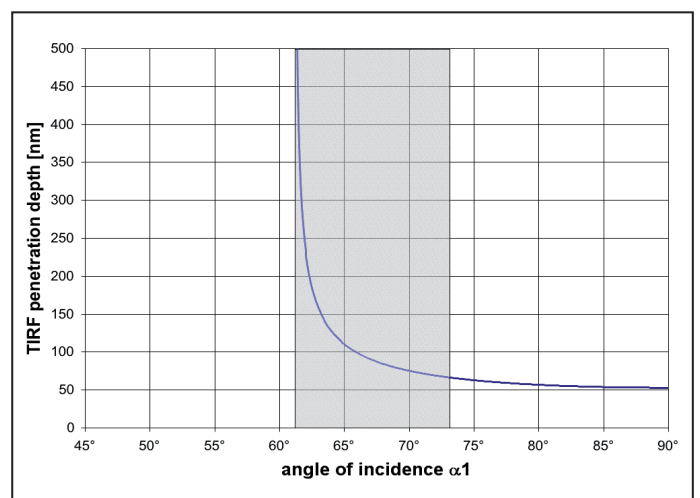


**Figure 5:** Penetration depth of the evanescent field as a function of the angle of incidence for  $\lambda_0 = 488\text{nm}$ ,  $n_1 = 1,518$ ,  $n_2 = 1,33$  and therefore resulting  $\alpha_g = 61,2^\circ$  (see paragraph 2). The hatched area represents the working range of the Zeiss-objective Alpha Plan Fluor 100x/1.45

penetration depth" in connection with microscopic resolution is imprecise. Mathematically seen the penetration depth concerns (see **figure 6**) the  $1/e$  value of the intensity of the light field at the interface. A penetration depth of 125 nm therefore does not mean that this is the maximum penetration depth of 'sufficient' excitation light to excite fluorophores. Many more deeply lying layers of the sample can also be excited. They are however seen only if the sensitivity of eye or camera is sufficient. The effective layer thickness of a TIRF image is thus determined also by the detection threshold as shown in **figure 6**. In addition the "expression level" has to be concerned as an independent parameter: the local concentration of fluorophores in the sample. If more deeply lying parts of the sample have a higher fluorophore concentration, that can compensate the effect of the weaker excitation.

## 5 Technical implementation

For the use of the TIRF effect in microscopy the use of lasers is favourable, because they can produce beams of parallel light rays<sup>1</sup> behind the objective. Chromatic errors of the illumination system can more easily be corrected for with narrow-band lasers, although alternative solutions also work with a conventional mercury arc lamp [5]. While other manufacturers of TIRF equipment make direct modifications to the microscope, Zeiss realized a solution with which laser illumination can be coupled using a slider, which is slid as a module into a standard slot of the microscope. **Figure 7** shows the so-called "TIRF slider" for the Zeiss Axiovert 200 microscope. Laser illumination is coupled using a polarization-maintaining monomode fiber (not shown in **figure 7**) from the right into the slider. A lens in the slider collimates the light and passes it on to a polarization-splitting cube. Since the laser light is polarized itself, it is reflected almost completely into the illumination path of the sample. At the same time conventional fluorescence excitation can take place by transmission through the cube. The conventional excitation experiences a 50% intensity loss from the polarization splitting cube which is typically not important. By a spindle screw the polarization-splitting cube is moveable few

<sup>1</sup> It is important that the laser beam at the position of the sample is a parallel bundle of light rays. If e.g. internal and outermost rays had clearly different angles of incidence, one side would already show total reflection, while at the other side would still observe Epi fluorescence. In **figure 2** a beam can be seen above the objective lens, which seems to be not parallel but focussed like an annulus. Within each differentially narrow angle segment of this annulus however the innermost and outermost rays are parallel to each other.

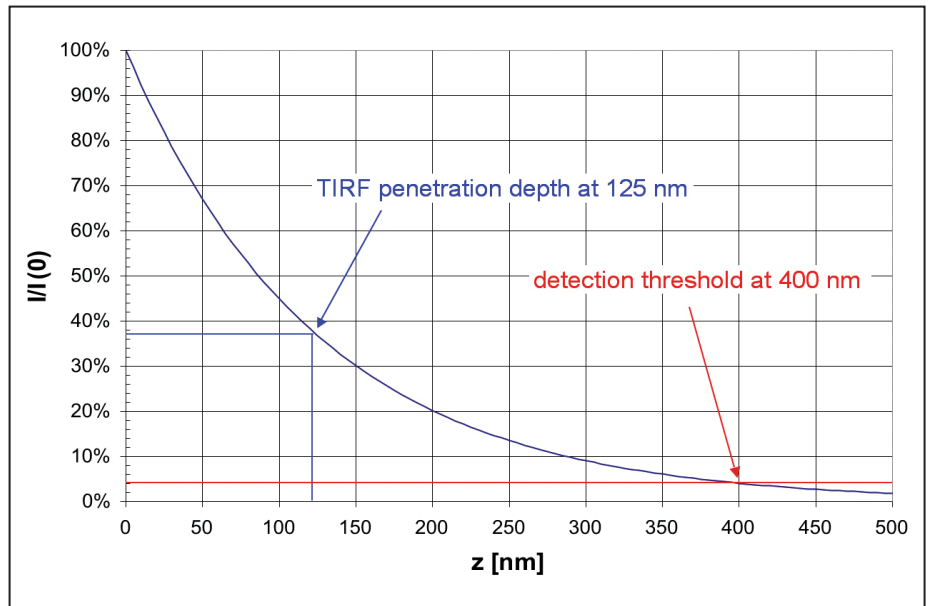


**Figure 6:** Relative intensity of the evanescent field versus depth. The different meaning of the penetration depth and the detection threshold is indicated (see text)

degrees around one of its lateral axes (perpendicular to the Z-axis), which leads in connection with the optical system to an adjustment of the angle of incidence  $\alpha_1$  over up to  $\pm 75^\circ$ . A grooved thumb screw (to be seen just behind the fiber coupling) permits the collimation of the laser beam behind the objective and an adjustment at different wavelengths and/or object heights.

## 6 Summary

The TIRF microscopy method, whose mathematical fundamentals were shown here, offers an extraordinarily high z-resolution to widefield microscopy by limiting fluorescence excitation to a very narrow, cover glass adjacent range of typically 100-200 nm depth. Since the necessary excitation optics can be realized in a modular slider, TIRF microscopy has now the potential to open new application areas with minimum expenditure.

## Acknowledgements:

I would like to thank Mr. Rainer Danz and Dr. Martin Voelcker for the critical examination of the manuscript. Additional thanks go to Dr. Juergen Klingauf (MPI for biophysical chemistry, Goettingen, [www.mpibpc.gwdg.de](http://www.mpibpc.gwdg.de)) for the supply of the illustrations of Phalloidin f-Aktin proteins.

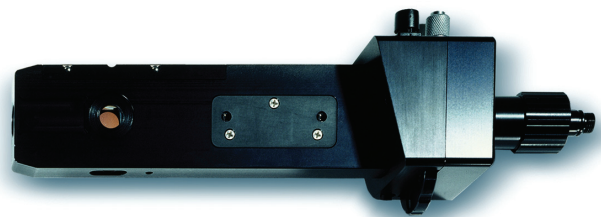


**Figure 7:** The TIRF slider for the Zeiss Axiovert 200 microscope

## Literature:

- [1] [www.zeiss.de/apotome](http://www.zeiss.de/apotome)
- [2] D. Axelrod, T.P. Burghardt, and N.L. Thompson (1984), *Total internal reflection fluorescence*, Annu. Rev. Biophys. Bioeng. **13**, 247-268
- [3] M. Toriumi and H. Masuhara (1991), *Time-resolved total internal reflection fluorescence spectroscopy: Principles, instruments and applications*, Spectrochim. Acta Rev. **14** (5), 353-377
- [4] [www.zeiss.de/tirf](http://www.zeiss.de/tirf)
- [5] [www.zeiss.de/sirf](http://www.zeiss.de/sirf)

## Corresponding author:

Dr. Matthias Kramer  
 Carl Zeiss MicroImaging GmbH  
 Development  
 Business Unit  
 Microscopy  
 Königsallee 9 - 21  
 37081 Göttingen  
 Germany  
 Tel. +49/551/5060-421  
 Fax +49/551/5060-650  
 eMail: [ma.kramer@zeiss.de](mailto:ma.kramer@zeiss.de)  
 Internet: [www.zeiss.de](http://www.zeiss.de)

